Analytical Approximate Solutions to Ground Track Adjustment for Responsive Space

GANG ZHANG
XIBIN CAO
Harbin Institute of Technology
Harbin, Heilongjiang, China

DANIELE MORTARI, Fellow, IEEE
Texas A&M University
College Station, Texas, USA

This paper analyzes a civilian or military responsive space mission, in which a specific Earth site needs to be visited in a short time. Approximate analytical solutions for single and dual coplanar impulsive maneuvers to move from initial circular/elliptical orbit to final circular/elliptical orbit whose ground track passes over the Earth site are provided. The problem is solved by computing the semimajor axis of the final orbit by setting the transfer time equal in terms of Kepler's equation and of Greenwich mean sidereal time (GMST). Using an unperturbed Keplerian model, a closed-form solution is obtained by solving a cubic polynomial. Then, by converting mean to osculating orbital elements, the linear J_2 perturbed exact overflight solutions are obtained for impulses and corresponding time instants. Moreover, the exact overflight solutions are extended when using a conical sensor. Several numerical examples with various initial and final orbits are provided to validate this approach.

Manuscript received August 31, 2014; revised July 30, 2015, December 16, 2015; released for publication December 17, 2015.

DOI. No. 10.1109/TAES.2016.140644.

Refereeing of this contribution was handled by M. Akella.

This work is supported in part by the National Natural Scientific Foundation of China (11402062, 61333003), and the Open Fund of National Defense Key Discipline Laboratory of Micro-Spacecraft Technology (HIT.KLOF.MST.201504).

Authors' addresses: G. Zhang, X. Cao, Harbin Institute of Technology, Research Center of Satellite Technology, Mailbox 3012, Science Park Building #B3, Yikuang street #2, Harbin, Heilongjiang 150080, China; D. Mortari, Texas A&M University, Aerospace Engineering, H.R. Bright Building, Rm. 746C, Ross Street - TAMU 314, College Station, TX 77843-3141. Corresponding author is G. Zhang, E-mail: (zhanggang@hit.edu.cn).

I. INTRODUCTION

Responsive space is important for civilian and military purposes. A quick satellite observation of a ground site where a natural disaster occurs (e.g., earthquake, forest fire, etc.) is of paramount importance to understand how to organize the emergency response operations. To give a practical example, the air traffic control with Malaysia Airlines Flight 370, carrying international passengers from Kuala Lumpur to Beijing, was lost on March 8, 2014. On March 11, 2014, China deployed 10 high-resolution satellites to sweep and survey the South China Sea to find leads that could help locate the airplane. This paper provides analytical tools to accomplish such service by changing a satellite ground track using inexpensive coplanar maneuvers. This is done by modifying the orbit shape (semimajor axis and/or eccentricity) of an assigned on-orbit satellite to make its ground track pass over a specific Earth site in a short time. The orbit shape is changed by in-plane maneuvers. Out-of-plane maneuvers (plane changes) are avoided as they are usually too expensive, especially for low Earth orbit (LEO) satellites.

The design of orbit ground tracks has been studied for many years. Repeated ground track orbit, also called resonant or compatible orbit, is particularly useful to periodically observe specific ground site(s) [1]. A repeated ground track condition with a simple and instructive mathematical description was precisely evaluated in [2]. To cover designated areas on the Earth, a semianalytical technique was proposed using orbital elements [3]. In addition, the original theory of Flower Constellations [4, 5] was built using compatible orbits. This theory then evolved into the Necklace theory of Flower Constellations [6] to minimize the number of satellites for real-time global/regional coverage.

To observe multiple sites (or border regions), genetic algorithms were used [7] for two types of objective functions: one is to optimize resolution and the other is to maximize the observation time. In particular, for the unperturbed Keplerian case, it has been proved that three arbitrary ground sites uniquely define a Keplerian orbit directly passing over them [8]. However, these orbital mechanics studies imply the deployment of a new satellite in orbit, while in this article, solutions to this observation problem are provided for the practical case of using an existing spacecraft in some assigned orbit.

The existing studies and results of ground track adjustments for a specific initial orbit can be classified in two distinct approaches: the first provides a solution for the minimum-fuel impulse to visit an assigned ground site within a prescribed time limit using numerical optimization algorithms, whereas the second provides a solution for an analytical approximation of the ground track variation under a given impulse or a given continuous thrust acceleration. For the first approach, a hybrid optimization algorithm using particle swarm optimization and differential evolution algorithms was proposed [9] to solve the ground track adjustment problem

by impulsive maneuvers for multiple satellites. In that study the objective function maximized the observation coverage time and minimized the orbit transfer cost. For the second approach, the ground-track reachability was quantified using impulsive or continuous propulsion based on initial orbit ΔV and available maneuvering time [10]. Under a given impulsive or continuous thrust, a numerical curve fitting function between terrestrial distance and propagating time was obtained. This function can be used to solve impulse and thrust magnitude for a given distance at assigned time. Moreover, a constant along-track low-thrust control algorithm was proposed based on a single equation of the time change between the maneuvering and reference ground tracks [11]. In these studies the required impulse or thrust magnitude was not obtained in an explicit form to visit an assigned ground site. Recently, an approximate analytical model was provided for the ground track variation under J_2 perturbations using a small tangential impulse on initial circular orbit [12].

The purpose of this paper is to derive analytical solutions for ground track adjustments to visit a user-specified ground site. Two tangential-impulse based approaches are proposed. The first one is a two-impulse approach to reach a circular final orbit, whereas the second uses a single impulse to get to an elliptical final orbit. Initial circular and elliptical orbits are both considered. Moreover, both cases of exact overflight and conical sensor are studied. The semimajor axis of the final orbit is analytically solved to obtain the required impulses and the corresponding time instants. In this analytical method, the linear J_2 perturbation is taken into account. However, drag, third-body, solar radiation pressure, and higher order gravitational perturbations are not included. This means that the analytic solutions provided should then be slightly refined using any existing software package able to include all perturbations, such as AGI-STK (Analytical Graphics' Satellite Tool Kit) or NASA-GMAT (General Mission Analysis Tool).

II. PROBLEM STATEMENT

Consider a LEO satellite with known orbital elements, available to perform impulsive maneuvers to change its ground track in order to pass over a given ground site S, specified by its longitude λ and latitude φ. Since plane change maneuvers (i.e., inclination or right ascension of ascending node) are usually expensive, in-plane impulses to adjust the ground track are considered. Two scenarios are analyzed: a two-impulse approach to a final circular orbit and a single-impulse approach to a final elliptical orbit. The velocity impulses are assumed to be aligned with the velocity vectors. This assumption, which has also been adopted in [10] for both impulsive and continuous thrusts, is made to maximize the orbital energy change.

The variables in the ground-track adjustment problem are the impulse times, positions, magnitudes, and directions. Considering all of them, the problem becomes very complicated and a numerical optimization technique must be used to solve it. To simplify the problem, the following assumptions are made: 1) a two-impulse approach to a final circular orbit and a single-impulse approach to a final elliptical orbit are considered, 2) the velocity impulses are assumed to be aligned with the velocity vectors, and 3) the impulse is applied at the initial time to simplify the problem or the apse to minimize the transfer costs.

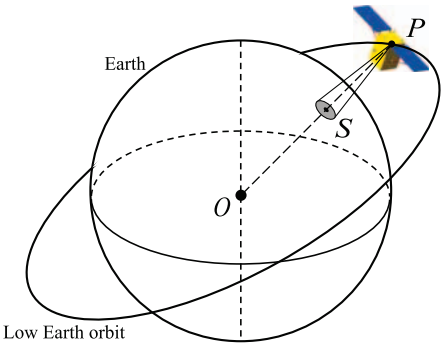

Fig. 1. Geometrical comprehension of ground track.

In this paper, two cases of exact overflight and bounded-side observation by the conical sensor are considered. The exact overflight case is considered first, followed by the conical sensor case. For the exact overflight case using planar orbit maneuver, the maximum latitude for the target site S coincides with the orbit inclination, while for the conical sensor case, the maximum latitude of the target site can be slightly greater than the orbit inclination.

In this paper the following nomenclature is adopted. Subscript 0 indicates the initial orbit, the true anomaly at initial time is denoted by f_{00}, and the initial argument of latitude is denoted by u_{00}. The orbital elements of the final orbit (whose ground track passes through S) have no subscripts, and the satellite point of the final orbit over the subsatellite point S is indicated by P (see Fig. 1). In addition, the true anomalies of the final orbit at initial time and at the satellite point P are indicated by f_0 and f_t, respectively. The corresponding arguments of latitude are indicated by u_0 and u_t, respectively. The case of initial equatorial orbit $i_0 = 0$ is excluded, as in this case, the problem cannot be solved if $\varphi \neq 0$ or no maneuver would be needed if $\varphi = 0$. Therefore, the $i_0 \neq 0$ case is assumed.

III. TWO-IMPULSE METHOD FOR EXACT OVERFLIGHT

In the ground-track adjustment problem, the initial time, the initial orbit, and the geographical coordinates of the target ground site are assigned. The solution consists of the impulses and the corresponding time instants. These quantities can be derived by computing the semimajor axis of the final orbit. In this section, the spacecraft is considered in an initial (circular or elliptical) orbit and a two-impulse maneuver is applied to reach a final circular orbit. The initial orbit, transfer orbit, and final orbit are all

coplanar. The Keplerian (two-body) model and the linear J_2 model are used to analyze the problem. Then, the solutions of the two impulses are obtained by considering a Hohmann-transfer maneuver.

A. Ground Track Calculation

Using unperturbed Keplerian orbit, the ground track is obtained by orbit propagation. This is done by evaluating the radius vector ($\boldsymbol{r}_\oplus$) in the Earth-centered Earth-fixed (ECEF) rotating frame. The expression of this vector at time t is

$$\boldsymbol{r}_\oplus = R_z(\alpha_G)\,\boldsymbol{r} = \frac{a(1-e^2)}{1+e\,\cos f} \times \begin{Bmatrix} \cos(\alpha_G-\Omega)\cos(\omega+f)+\sin(\alpha_G-\Omega)\sin(\omega+f)\cos i \\ -\sin(\alpha_G-\Omega)\cos(\omega+f)+\cos(\alpha_G-\Omega)\sin(\omega+f)\cos i \\ \sin(\omega+f)\sin i \end{Bmatrix} \tag{1}$$

where $R_z\ (\alpha_G)$ is the transformation matrix moving from Earth centered inertial (ECI) to ECEF, $\boldsymbol{r}$ is the position vector in the ECI frame, a the semimajor axis, e the eccentricity, i the inclination, ω the argument of perigee, Ω the right ascension of ascending node, f the true anomaly, and α_G is the Greenwich Mean Sidereal Time (GMST) computed at time t. Equation (1) is specified for elliptical orbits. However, it can also be adopted for circular orbits by setting $e = 0$ and replacing $\omega + f$ with argument of latitude u.

The site (geodetic) latitude $\varphi_k \in [-\pi/2, \pi/2]$ can be approximated by the declination (geocentric latitude), which is expressed by

$$\sin\varphi_k \approx \frac{\boldsymbol{r}_\oplus(3)}{r} = \sin u\ \sin i \tag{2}$$

The geographical longitude $\lambda_k \in [-\pi, \pi)$ is provided by

$$\sin\lambda_k = \frac{\boldsymbol{r}_\oplus(2)}{\sqrt{[\boldsymbol{r}_\oplus(1)]^2+[\boldsymbol{r}_\oplus(2)]^2}} = \frac{-\sin(\alpha_G-\Omega)\cos u+\cos(\alpha_G-\Omega)\sin u\cos i}{\sqrt{1-\sin^2 u\sin^2 i}} \tag{3a}$$

$$\cos\lambda_k = \frac{\boldsymbol{r}_\oplus(1)}{\sqrt{[\boldsymbol{r}_\oplus(1)]^2+[\boldsymbol{r}_\oplus(2)]^2}} = \frac{\cos(\alpha_G-\Omega)\cos u+\sin(\alpha_G-\Omega)\sin u\cos i}{\sqrt{1-\sin^2 u\sin^2 i}} \tag{3b}$$

For any assigned orbit, the orbit elements are computed by orbit propagation. Then, (2) and (3) provide the corresponding geographical longitude and latitude. This is done not only for the two-impulse final circular orbit.

B. Keplerian Model

In general, the ground track of the initial orbit does not pass over the target site S (longitude λ, latitude φ). To compute the required impulsive maneuver(s) for the desired ground track, the semimajor axis of the final orbit must be solved. The true anomaly f_t of the final orbit when the satellite passes over the site S, can be computed using (2), i.e.,

$$f_t = \sin^{-1}\left(\frac{\sin\varphi}{\sin i}\right) - \omega \tag{4}$$

The two solutions for f_t provided by (4) are associated with the ascending and descending orbit parts, respectively. The argument of latitude at P is $u_t = \omega + f_t = \sin\varphi/\sin i$. Equation (3) can be rewritten in matrix form

$$\begin{bmatrix} -\cos(\omega+f_t) & \sin(\omega+f_t)\cos i \\ \sin(\omega+f_t)\cos i & \cos(\omega+f_t) \end{bmatrix} \begin{Bmatrix} \sin(\alpha_{Gt}-\Omega) \\ \cos(\alpha_{Gt}-\Omega) \end{Bmatrix} = \sqrt{1-\sin^2(\omega+f_t)\sin^2 i}\ \begin{Bmatrix} \sin\lambda \\ \cos\lambda \end{Bmatrix} \tag{5}$$

Now, combining (2) and (5) we obtain

$$\begin{Bmatrix} \sin(\alpha_{Gt}-\Omega) \\ \cos(\alpha_{Gt}-\Omega) \end{Bmatrix} = \frac{-1}{\sqrt{1-\sin^2\varphi}} \begin{bmatrix} \cos(\omega+f_t) & -\sin(\omega+f_t)\cos i \\ -\sin(\omega+f_t)\cos i & -\cos(\omega+f_t) \end{bmatrix} \times \begin{Bmatrix} \sin\lambda \\ \cos\lambda \end{Bmatrix} \triangleq \begin{Bmatrix} c_1 \\ c_2 \end{Bmatrix} \tag{6}$$

Equation (6) allows us to compute the GMST angle at satellite point P (or subsatellite point S),

$$\alpha_{Gt} = \Omega + \text{atan2}(c_1, c_2) \tag{7}$$

Then the flight time from initial time to the time when the satellite reaches the point P, is

$$t_G = \frac{(\alpha_{Gt}-\alpha_{G0})+2\pi(D-1)}{\omega_\oplus} \tag{8}$$

where $\omega_\oplus = 7.2921158553\ 10^{-5}$ rad/s is the rotation rate of the Earth, D is the number of days, and α_{G0} is the GMST at initial time.

The argument of latitude at P on the final circular orbit is obtained from (4). If u_0 is the initial argument of latitude on the final orbit, then the flight time using circular final orbit (from impulse point to satellite point P) is obtained from Kepler's equation

$$t_K = \sqrt{\frac{a^3}{\mu}}\,(u_t - u_0 + 2\pi N_R) \tag{9}$$

where μ is the gravity parameter and N_R the number of orbit revolutions. The argument of latitude at P is $u_t = \sin\varphi\ /\sin i_0$.

Finally, by equating (8) and (9) (by setting $t_G = t_K$), the semimajor axis of the final circular orbit is computed as

$$a = \left\{\frac{[(\alpha_{Gt}-\alpha_{G0})+2\pi(D-1)]\sqrt{\mu}}{(u_t-u_0+2\pi N_R)\,\omega_\oplus}\right\}^{2/3} \tag{10}$$

where the number of orbital period N_R is selected to minimize the ΔV_{tot} cost. This selection determines the

optimal (minimum energy) semimajor axis. The admissible values of N_R are $\{1, 2, \cdots, N_{R_{\max}}\}$. In our numerical tests, the value of $N_{R_{\max}}$ is derived using a 200 km altitude circular orbit, i.e., $N_{R_{\max}} = \lfloor 86,400\, D/(2\pi\sqrt{(R_\oplus + 200\,\text{km})^3/\mu})\rfloor$, where $R_\oplus = 6{,}378.14$ km is the Earth's radius.

Once the semimajor axis of the final circular orbit is obtained, for the initial circular orbit case, a Hohmann transfer between two circular orbits is adopted. In this case, the total cost of the two impulses is

$$\Delta V_{\text{tot}} = \sqrt{\frac{\mu}{a_0}}\left|\sqrt{\frac{2\,a}{a_0+a}} - 1\right| + \sqrt{\frac{\mu}{a}}\left|1 - \sqrt{\frac{2\,a_0}{a_0+a}}\right| \tag{11}$$

If the initial orbit is elliptical, the 180° Hohmann-like transfer (from elliptical to circular) is adopted. Two cases appear:

1) First impulse at the apogee of the initial orbit. In this case, using the velocity-magnitude expression, $v = \sqrt{\mu(2/r - 1/a_t)}$ for semimajor axis a_t, the total cost is expressed as

$$\Delta V_{\text{tot}} = \sqrt{\frac{\mu}{a_0(1+e_0)}}\left|\sqrt{\frac{2\,a}{a_0(1+e_0)+a}} - \sqrt{1-e_0}\right| + \sqrt{\frac{\mu}{a}}\left|1 - \sqrt{\frac{2a_0(1+e_0)}{a_0(1+e_0)+a}}\right| \tag{12}$$

2) First impulse at the perigee of the initial orbit. In this case the total cost becomes

$$\Delta V_{\text{tot}} = \sqrt{\frac{\mu}{a_0(1-e_0)}}\left|\sqrt{\frac{2a}{a_0(1-e_0)+a}} - \sqrt{1+e_0}\right| + \sqrt{\frac{\mu}{a}}\left|1 - \sqrt{\frac{2a_0(1-e_0)}{a_0(1-e_0)+a}}\right| \tag{13}$$

In both cases, the second impulses are at a 180° transfer angle. Reference [13] has shown that the ΔV_{tot} cost obtained using first impulse at apogee is convenient if $a < a_0\,(1 + e_0)$, whereas the first impulse applied at perigee is preferable if $a > a_0\,(1 + e_0)$. However, the difference between both cases is small when $a \notin [a_0\,(1 - e_0),\, a_0\,(1 + e_0)]$.

Fig. 2 shows the total costs of first impulse at apogee or perigee for a given initial elliptical orbit with $a_0 = R_\oplus + 800$ km and $e_0 = 0.05$, and for altitudes of the final circular orbit ranging from $h = 300$ km to $h = 1200$ km. This figure clearly shows that the cost difference between these two approaches is small (the maximum difference is about 0.02%) when $a \notin [a_0\,(1 - e_0),\, a_0\,(1 + e_0)]$, and the minimum-fuel solution occurs at $a = a_0\,(1 + e_0)$. Therefore, for initial elliptical orbit, the first impulse at apogee is adopted even if $a > a_0\,(1 + e_0)$. Then, the cost of the two impulses is obtained by (12).

In the two-impulse method, the final semimajor axis is $a \approx a_0$ for initial circular orbit and $a \approx a_0(1 + e_0)$ for initial elliptical orbit. Therefore, the optimal N_R can be

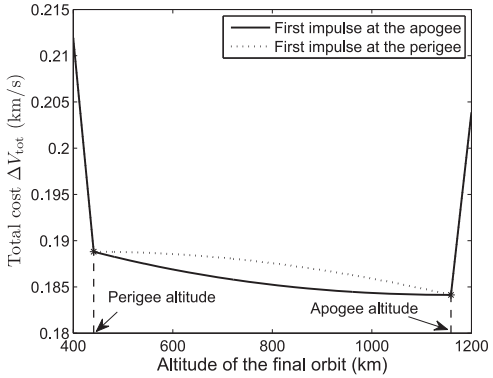

Fig. 2. Cost comparison for first impulse at perigee and apogee.

estimated as

$$N_{R\text{opt}} = \frac{1}{2\pi}\left(t_G\sqrt{\frac{\mu}{a_0^3(1+e_0)^3}} - u_t + u_{00}\right) \tag{14}$$

for both initial circular and elliptical orbits. The value of $N_{R\text{opt}}$ may not be an integer, then "ceil" and "floor" functions can be used to find the closest integer value.

In summary, in the two-impulse final-circular-orbit approach, if the initial orbit is circular, then a Hohmann transfer is applied with the first impulse occurring at the initial time. If the initial orbit is elliptical, then the first impulse of a Hohmann-like transfer is applied at apogee.

C. Linear J_2 Model

The Earth's oblateness perturbation on orbits (J_2 effect) is a slow effect as compared with the orbital period. For this reason, the J_2 effect cannot be ignored when the flight time is several days. Under the linear J_2 perturbation, a, e, and i remain constant (no secular drifts), whereas ω, Ω, and M change according to [1]

$$\begin{cases} \dot{\omega}_{J_2} = C_{J_2}(2 - \frac{5}{2}\sin^2 i)/(1-e^2)^2 \\ \dot{\Omega}_{J_2} = -C_{J_2}\cos i/(1-e^2)^2 \\ \dot{M}_{J_2} = C_{J_2}(1 - \frac{3}{2}\sin^2 i)/(1-e^2)^{3/2} \end{cases} \tag{15}$$

where M is the mean anomaly, $C_{J_2} = 1.5\,J_2\,R_\oplus^2\sqrt{\mu}\,a^{-7/2}$, and $J_2 = 1.082627\ 10^{-3}$. Note that $\dot{\omega}_{J_2}$, $\dot{\Omega}_{J_2}$, and $\dot{M}_{J_2}$ are all functions of a, which is obtained from (10) for the Keplerian model.

Under the linear J_2 perturbation, the varying orbital elements at time t are

$$\begin{cases} \omega_t = \omega + \dot{\omega}_{J_2}\,t \\ \Omega_t = \Omega + \dot{\Omega}_{J_2}\,t \\ M_t = M_0 + nt + \dot{M}_{J_2}\,t \end{cases} \tag{16}$$

where $n = \sqrt{\mu/\bar{a}^3}$ is the mean motion, and where $\bar{a}$ is the mean semimajor axis. Let u_0 be the initial argument of latitude of the final orbit. Then, the final argument of latitude at time t becomes

$$u_t = u_0 + t\sqrt{\frac{\mu}{\bar{a}^3}} - 2\pi\,N_R + (\dot{M}_{J_2} + \dot{\omega}_{J_2})\,t \tag{17}$$

The argument of latitude can then be used in Kepler's equation to compute the flight time

$$t_{K_{J_2}} = \frac{(u_t - u_0) + 2\pi N_R}{\dot{M}_{J_2} + \dot{\omega}_{J_2} + \sqrt{\mu/\bar{a}^3}} \tag{18}$$

Since tangential impulses do not change the orbit plane ($i = i_0$ and $\Omega = \Omega_0$), the flight time can also be derived from the GMST variation as

$$t_{G_{J_2}} = \frac{\Omega_0 + \text{atan2}(c_1, c_2) - \alpha_{G0} + 2\pi(D-1)}{\omega_\oplus - \dot{\Omega}_{J_2}} \tag{19}$$

Now, by setting $t_{K_{J_2}} = t_{G_{J_2}}$, the mean semimajor axis of the final orbit under the linear J_2 perturbation is

$$\bar{a} = \mu^{1/3}\left\{\frac{[(u_t - u_0) + 2\pi N_R](\omega_\oplus - \dot{\Omega}_{J_2})}{\Omega_0 + \text{atan2}(c_1, c_2) - \alpha_{G0} + 2\pi(D-1)} - \dot{M}_{J_2} - \dot{\omega}_{J_2}\right\}^{-2/3} \tag{20}$$

The transformation from mean into osculating orbital elements [14] can then be performed to compute the required impulses given by (12).

The final orbit computed from the mean semimajor axis evaluated using (20) has the ground track passing over the site S. For the two-impulse approach, the solution is valid for both circular and elliptical initial orbits. However, a transfer orbit arc connecting initial and final orbits is required. The use of Hohmann transfer is a simple but not general solution. In fact, this problem can be solved as a rendezvous problem. In this case, the satellite on the initial orbit performs a rendezvous to a "fictitious satellite" on the final orbit. Then, after the final (second) impulse of the rendezvous, the ground track of the satellite orbit is the same as that of the final circular orbit. This optimal two-impulse orbital rendezvous problem can be solved using a numerical optimization technique [15].

D. Initial Circular Orbit

The previous subsection proposes a method to compute the final orbit but not to evaluate the transfer orbit. This is provided in this subsection by a simple two-impulse Hohmann-transfer with the linear J_2 perturbation.

The total flight time t_K, obtained by Kepler's equation, is related to the Hohmann-transfer arc through different semimajor axes of the transfer and final orbits. However, the flight time t_G, obtained by the GMST variation using (8), is independent from the Hohmann-transfer arc, even though $t_{G_{J2}}$ is slightly influenced by the transfer orbit because $\dot{\Omega}_{J_2}$ is a function of a, as shown by (19).

For the initial circular orbit, the first impulse is at the initial time while the second impulse is at a 180° transfer angle, where the argument of latitude of the circular final orbit becomes $u_{00} + \pi$. Therefore, using the Keplerian model, the total flight time from initial time to point P is

$$t_K = \pi\sqrt{\frac{(a_0 + a)^3}{8\mu}} + (u_t - u_{00} - \pi + 2\pi N_R)\sqrt{\frac{a^3}{\mu}} \tag{21}$$

where the first term is the transfer time t_H for the Hohmann-transfer arc. Since a is close to a_0, using the first-order Taylor series expansion we can write

$$\left(\frac{a_0 + a}{2}\right)^{3/2} = a^{3/2}\left[1 + \frac{1}{2}\left(\frac{a_0}{a} - 1\right)\right]^{3/2} \approx a^{3/2}\left[1 + \frac{3}{4}\left(\frac{a_0}{a} - 1\right)\right] \approx \frac{1}{4}a^{3/2} + \frac{3}{4}a_0\, a^{1/2} \tag{22}$$

Substituting (22) into (21) yields a cubic equation in terms of $\sqrt{a}$

$$\left[\frac{\pi}{4} + (u_t - u_{00} - \pi + 2\pi N_R)\right](\sqrt{a})^3 + \frac{3\pi}{4}a_0\sqrt{a} - t_G\sqrt{\mu} = 0 \tag{23}$$

where t_G is obtained by (8). The semimajor axis a of the final orbit is then obtained in a closed form as this depressed cubic equation has a unique real root.

When the J_2 perturbation is considered, the contributions due to the secular drifting rates $\dot{\omega}_{J_2}$, $\dot{\Omega}_{J_2}$, and $\dot{M}_{J_2}$ must be included in the flight-time computation. Using (18), the total flight time under the J_2 effect from initial time to point P is

$$t_{K_{J_2}} = \chi_H\,\pi\sqrt{\frac{(a_0 + \bar{a})^3}{8\mu}} + \chi\,(u_t - u_{00} - \pi + 2\pi N_R)\sqrt{\frac{\bar{a}^3}{\mu}} \tag{24}$$

where the new parameter (χ) is defined as

$$\chi \triangleq \left[1 + (\dot{M}_{J_2} + \dot{\omega}_{J_2})\sqrt{\bar{a}^3/\mu}\right]^{-1} \tag{25}$$

and χ_H is obtained by replacing a and e in (25) with $a_H = (a + a_0)/2$ and $e_H = |a - a_0|/(a + a_0)$, respectively. The subscript H identifies quantities of the Hohmann-transfer arc. For the final circular orbit, $e = 0$ is set. Note that, χ and χ_H are functions of $\bar{a}$. The mean semimajor axis $\bar{a}$ of the final orbit cannot be obtained in a closed form from (24). However, the difference of the semimajor axes obtained by the Keplerian model and the J_2 model should be small. This allows us to obtain an approximate expression for (24),

$$t_{K_{J_2}} \approx \chi_{Hs}\,\pi\sqrt{\frac{(a_0 + \bar{a})^3}{8\mu}} + \chi_s\,(u_t - u_{00} - \pi + 2\pi N_R)\sqrt{\frac{\bar{a}^3}{\mu}} \tag{26}$$

where χ_s and χ_{Hs} are obtained using the Keplerian solution (a_s) in (23). The value of a_s is also used to calculate $\dot{\omega}_{J_2}$, $\dot{\Omega}_{J_2}$, and $\dot{M}_{J_2}$. Finally, a cubic equation of $\sqrt{\bar{a}}$, similar to (23), can be obtained,

$$\left[\frac{\pi}{4}\chi_{Hs} + \chi_s(u_t - u_{00} - \pi + 2\pi N_R)\right](\sqrt{\bar{a}})^3 + \frac{3\pi}{4}\chi_{Hs}a_0\sqrt{\bar{a}} - t_{G_{J_2}}\sqrt{\mu} = 0 \tag{27}$$

and, therefore, a closed-form solution for the mean semimajor axis of the final orbit under the J_2 effect is obtained. The value of a is then transformed from mean value ($\bar{a}$), allowing us to compute the two impulses of the Hohmann transfer using (11).

For each admissible value of N_R, the semimajor axes of the final orbit for the Keplerian model and for the J_2 model can be obtained using (23) and (27), respectively. The minimum-energy solution with the optimal N_R (near to $N_{R\text{opt}}$) can then be identified.

To summarize the procedure, given the initial time, initial circular orbit, and assigned ground site S, the proposed process for a two-impulse initial circular orbit is as follows.

1) Using the Keplerian model, the semimajor axis a_s of the final orbit is obtained using (23), where t_G is obtained from (8).

2) Compute $\dot{\omega}_{J_2}$, $\dot{\Omega}_{J_2}$, and $\dot{M}_{J_2}$ using (15) and the Keplerian semimajor axis a_s; then, compute $t_{G_{J_2}}$ using (19) and χ_s, χ_{Hs} using (25).

3) To include the J_2 perturbation, compute the mean semimajor axis $\bar{a}$ of the final orbit using (27).

4) The other orbital elements of the final orbit are identical to those of the initial orbit. Set these orbital parameters as mean orbital elements, and transform them into osculating elements.

5) Compute the two impulses for the Hohmann transfer using (11). The first impulse is at the initial time while the second impulse is displaced by a 180° transfer angle. The second impulse time is $t_2 = t_H$ which is obtained using the first term of (24).

6) The minimum ΔV_{tot} solution is then obtained using steps 1 through 5 for all the admissible values of N_R.

E. Initial Elliptical Orbit

When the initial orbit is elliptical, the first impulse of the Hohmann-like transfer occurs at the apogee, while the second impulse occurs at a 180° transfer angle where the true anomaly is 0. If the initial true anomaly is $f_{00} \neq \pi$, there will be an initial coasting arc before the first impulse. Using the Keplerian model the argument of latitude of the final orbit at the second impulse is w_0. The total flight time from initial time to point P is

$$t_K = (\pi - M_{00})\sqrt{\frac{a_0^3}{\mu}} + \pi\sqrt{\frac{[a_0(1+e_0)+a]^3}{8\mu}} + (u_t - \omega_0 + 2\pi N_R)\sqrt{\frac{a^3}{\mu}} \tag{28}$$

where the first and second terms indicate the initial coasting time t_{coasting} and the Hohmann transfer time t_H, respectively. Since $a \approx a_0\,(1 + e_0)$ and $t_K = t_G$, a cubic equation, similar to (23), is obtained

$$\left[\frac{\pi}{4} + (u_t - \omega_0 + 2\pi N_R)\right](\sqrt{a})^3 + \frac{3\pi}{4}a_0(1+e_0)\sqrt{a} - \left[t_G\sqrt{\mu} - (\pi - M_{00})\sqrt{a_0^3}\right] = 0 \tag{29}$$

This equation provides a closed-form solution of a for the Keplerian model.

For the perturbed J_2 model, the initial coasting time from initial position to the impulse time (apogee) is independent from the final orbit. Therefore, numerical methods are used to obtain an exact value for the initial coasting time t_{coasting}. This value can be used to replace the first term in (28). Then, the orbital elements at the apogee can be considered as those of the "new" initial orbit. Therefore, the total flight time under J_2 perturbation is

$$t_{K_{J_2}} \approx t_{\text{coasting}} + \chi_{Hs}\pi\sqrt{\frac{[a_0(1+e_0)+\bar{a}]^3}{8\mu}} + \chi_s(u_t - \omega_0 + 2\pi N_R)\sqrt{\frac{\bar{a}^3}{\mu}} \tag{30}$$

where χ_s is obtained using the Keplerian solution (a_s) provided by (29), and χ_{Hs} is computed using the semimajor axis $a_{Hs} = [a_s + a_0\,(1 + e_0)]/2$ and the eccentricity $e_{Hs} = |a_s - a_0\,(1 + e_0)|/[a_s + a_0\,(1 + e_0)]$. The value of a_s is also used to compute $\dot{\omega}_{J_2}$, $\dot{\Omega}_{J_2}$, and $\dot{M}_{J_2}$. Similarly to (29), the final mean semimajor axis $\bar{a}$ under J_2 perturbation is obtained from

$$\left[\frac{\pi}{4}\chi_{Hs} + \chi_s(u_t - \omega_0 + 2\pi N_R)\right](\sqrt{\bar{a}})^3 + \frac{3\pi}{4}\chi_{Hs}a_0(1+e_0)\sqrt{\bar{a}} - (t_{G_{J_2}} - t_{\text{coasting}})\sqrt{\mu} = 0 \tag{31}$$

The summary of the steps used for the two-impulse initial elliptical orbit case is as follows.

1) For the Keplerian model, compute the semimajor axis a_s of the final orbit using (29), where t_G is obtained by (8).

2) Compute $\dot{\omega}_{J_2}$, $\dot{\Omega}_{J_2}$, and $\dot{M}_{J_2}$ using (15) and the Keplerian semimajor axis a_s; then, compute $t_{G_{J_2}}$ using (19) and [χ_s, χ_{Hs}] using (25).

3) For the perturbed J_2 model, the initial coasting time, t_{coasting}, is computed using numerical methods. The orbital elements at the apogee constitute the "new" initial orbit. The final mean semimajor axis $\bar{a}$ is then computed using (31).

4) The other orbital elements of the final orbit are the same as those of the initial orbit at t_{coasting}. Set these orbital parameters as mean orbital elements, and then transform them into osculating elements.

5) The two impulses of the Hohmann-like transfer are obtained using (12). The first impulse is performed at the apogee of the initial orbit, i.e., at $t_1 = t_{\text{coasting}}$, while the second impulse occurs at a 180° transfer angle. The second impulse time, obtained using (30), is $t_2 = t_{\text{coasting}} + t_H$.

6) The minimum ΔV_{tot} solution is obtained using steps 1 through 5 for all the admissible values of N_R.

IV. SINGLE-IMPULSE METHOD FOR EXACT OVERFLIGHT

The previous section provides a two-impulse approach using a circular final orbit to visit the target site S. This section provides a single-impulse approach with an elliptical final orbit to visit the site. Using a single impulse the initial orbit is directly changed into the final orbit. Therefore, there is no need to consider initial coasting arc and transfer orbit arc. Two cases of initial circular and elliptical orbits are considered.

A. Initial Circular Orbit

The purpose of this section is to derive the semimajor axis of the final elliptical orbit. To obtain the flight time using Kepler's equation, the eccentric anomaly is expressed in terms of the true anomaly as

$$E = 2\arctan\left(\sqrt{\frac{1-e}{1+e}}\tan\frac{f}{2}\right) \tag{32}$$

The final orbit is considered with small eccentricity, $e \ll 1$. Clearly, this assumption also requires a small tangential impulse. By performing the Taylor series expansion of (32) and dropping out all the terms higher than the linear we obtain

$$E \approx f - e\sin f \tag{33}$$

Then, for a small value of eccentricity, the mean anomaly can be expressed as

$$M = E - e\sin E \approx f - 2e\sin f \tag{34}$$

Consider an initial circular orbit in which an impulse is applied along the velocity-vector direction at location u_{00}. If the impulse is positive ($\Delta V > 0$), the location of the impulse becomes the perigee of the final orbit (true anomaly $f_0 = 0$); whereas if the impulse is negative ($\Delta V < 0$), it becomes the apogee ($f_0 = \pi$). Therefore, for the Keplerian model, using the expression given in (34), Kepler's equation is written as

$$f_t - 2e\sin f_t + 2\pi N_R + [\text{sign}(\Delta V) - 1]\frac{\pi}{2} = t_K\sqrt{\frac{\mu}{a^3}} \tag{35}$$

where f_t is obtained from (4), and where $\omega = u_{00}$ if $\Delta V > 0$ and $\omega = u_{00} + \pi$ if $\Delta V < 0$.

Using a tangential impulse, Lagrange planetary equations imply $\Delta i = 0$ and $\Delta\Omega = 0$, while the variations of semimajor axis and eccentricity are

$$\Delta a \approx 2\sqrt{\frac{a_0^3}{\mu}}\,\Delta V \tag{36}$$

and

$$\Delta e \approx \text{sign}(\Delta V)\,2\sqrt{\frac{a_0}{\mu}}\Delta V \tag{37}$$

Therefore, the eccentricity e can be expressed in terms of a

$$e = \Delta e \approx \text{sign}(\Delta V)\,\frac{\Delta a}{a_0} = \text{sign}(\Delta V)\left(\frac{a}{a_0} - 1\right) \tag{38}$$

Substituting (38) into (35) yields

$$f_t - \text{sign}(\Delta V)\,2\left(\frac{a}{a_0} - 1\right)\sin f_t + 2\pi N_R + [\text{sign}(\Delta V) - 1]\frac{\pi}{2} = t_K\sqrt{\frac{\mu}{a^3}} \tag{39}$$

By setting $t_K = t_G$, a fifth-order equation in terms of $\sqrt{a}$ is then obtained. The root is then computed by numerical methods as a closed-form solution of the fifth-order algebraic equation does not exist. Instead of using the expression provided by (38), the eccentricity can be approximated as

$$e \approx \text{sign}(\Delta V)\left(1 - \frac{a_0}{a}\right) \tag{40}$$

Now, substituting (40) in (35) we obtain

$$f_t - \text{sign}(\Delta V)\,2\left(1 - \frac{a_0}{a}\right)\sin f_t + 2\pi N_R + [\text{sign}(\Delta V) - 1]\frac{\pi}{2} = t_K\sqrt{\frac{\mu}{a^3}} \tag{41}$$

from which the following cubic algebraic equation in terms of $\sqrt{a}$ is obtained

$$\left\{f_t + 2\pi N_R - \text{sign}(\Delta V)\,2\sin f_t + [\text{sign}(\Delta V) - 1]\frac{\pi}{2}\right\} \times (\sqrt{a})^3 + \text{sign}(\Delta V)\,2a_0\sin f_t\sqrt{a} - t_G\sqrt{\mu} = 0 \tag{42}$$

This equation is then solved in a closed form. For each value of N_R, a corresponding value of a is obtained. The optimal a is then identified as the one minimizing $|a - a_0|$, because (36) highlights a linearity between ΔV and Δa. Therefore, in this single-impulse approach, the optimal N_R is estimated using (14), for both circular and elliptical initial orbit cases.

When the linear J_2 perturbation is considered, the Kepler equation becomes

$$f_t - 2e\sin f_t + 2\pi N_R + [\text{sign}(\Delta V) - 1]\frac{\pi}{2} = t_{K_{J_2}}\sqrt{\frac{\mu}{\bar{a}^3}} + (\dot{M}_{J_2} + \dot{\omega}_{J_2})t_{K_{J_2}} \tag{43}$$

By setting $t_{K_{J_2}} = t_{G_{J_2}}$ and proceeding as before, this equation can be transformed into a cubic algebraic equation in terms of $\sqrt{\bar{a}}$

$$\{f_t + 2\pi N_R + [\text{sign}(\Delta V) - 1]\frac{\pi}{2} - \text{sign}(\Delta V)\,2\sin f_t - (\dot{M}_{J_2} + \dot{\omega}_{J_2})t_{G_{J_2}}\}(\sqrt{\bar{a}})^3 + \text{sign}(\Delta V)\,2a_0\sin f_t\sqrt{\bar{a}} - t_{G_{J_2}}\sqrt{\mu} = 0 \tag{44}$$

where $t_{G_{J_2}}$ is obtained using (19).

Once the mean semimajor axis $\bar{a}$ of the final orbit is obtained, then it is converted into the osculating value.

Using the osculating value the impulse is

$$\Delta V = \sqrt{\mu\left(\frac{2(1+e_0\cos f_{00})}{p_0} - \frac{1}{a}\right)} - \sqrt{\frac{\mu}{p_0}(1+e_0^2+2e_0\cos f_{00})} \tag{45}$$

where $p = a(1-e^2)$ is the semiparameter. Note that (45) is valid for both circular and elliptical initial orbit cases.

The process for the single-impulse initial circular orbit is summarized as follows.

1) When using the Keplerian model, f_t is obtained using (4), where $\omega = u_{00}$ if $\Delta V > 0$ and $\omega = u_{00} + \pi$ if $\Delta V < 0$. The semimajor axis a_s of the final orbit is then computed using (42), where t_G is obtained from (8).

2) The derivatives, $\dot{\omega}_{J_2}, \dot{\Omega}_{J_2}$, and $\dot{M}_{J_2}$, are computed using (15) and the Keplerian semimajor axis a_s. Then $t_{G_{J_2}}$ is computed using (19).

3) For the perturbed J_2 model, the mean semimajor axis $\bar{a}$,of the final orbit is computed using (44).

4) The eccentricity e is computed using (40), and ω and f_t are obtained using step 1, and $i = i_0$ and $\Omega = \Omega_0$. These orbital parameters are mean orbital elements. They must then be converted into osculating elements.

5) The tangential impulse (positive or negative) at the initial time is obtained using (45).

6) The minimum ΔV_{tot} solution is then obtained by looping steps 1 through 5 for all admissible values of N_R.

B. Initial Elliptical Orbit

Using an initial elliptical orbit and a tangential impulse ΔV, Lagrange planetary equations give $\Delta i = 0$ and $\Delta\Omega = 0$, while the variations of other orbital elements can be approximated as

$$\Delta a \approx \frac{2}{n_0\sqrt{1-e_0^2}}\Delta V[e_0\sin f_{00}\sin\gamma_{00} + (1+e_0\cos f_{00})\cos\gamma_{00}] \tag{46}$$

$$\Delta e \approx \frac{\sqrt{1-e_0^2}}{n_0 a_0}\Delta V[\sin f_{00}\sin\gamma_{00} + (\cos E_{00}+\cos f_{00})\cos\gamma_{00}] \tag{47}$$

$$\Delta\omega \approx \frac{\sqrt{1-e_0^2}}{n_0 a_0 e_0}\Delta V\left[-\cos f_{00}\sin\gamma_{00} + \frac{2+e_0\cos f_{00}}{1+e_0\cos f_{00}}\sin f_{00}\cos\gamma_{00}\right] \tag{48}$$

$$\Delta M \approx -\frac{1-e_0^2}{n_0 a_0 e_0}\Delta V\left[\left(\frac{2e_0}{1+e_0\cos f_{00}} - \cos f_{00}\right)\sin\gamma_{00} + \frac{2+e_0\cos f_{00}}{1+e_0\cos f_{00}}\sin f_{00}\cos\gamma_{00}\right] \tag{49}$$

where E_{00} is the eccentric anomaly at initial time, and where the initial flight-path angle γ_{00} is obtained as

$$\gamma_{00} = \arctan\left(\frac{e_0\sin f_{00}}{1+e_0\cos f_{00}}\right) \tag{50}$$

Using (46) and (47), the eccentricity variation is linearly related to the semimajor axis variation by the equation

$$\Delta e \approx \frac{1-e_0^2}{2a_0}\frac{\cos(f_{00}-\gamma_{00})+\cos E_{00}\cos\gamma_{00}}{e_0\cos(f_{00}-\gamma_{00})+\cos\gamma_{00}}\Delta a \tag{51}$$

This equation allows us to express the eccentricity of the final orbit in terms of the final semimajor axis a as

$$e \approx e_0 + \frac{1-e_0^2}{2}\frac{\cos(f_{00}-\gamma_{00})+\cos E_{00}\cos\gamma_{00}}{e_0\cos(f_{00}-\gamma_{00})+\cos\gamma_{00}}\left(\frac{a}{a_0}-1\right) \tag{52}$$

Similarly, by combining (46) and (48), the argument of perigee of the final orbit is

$$\omega \approx \omega_0 + \frac{(1-e_0^2)/(2e_0)}{e_0\cos(f_{00}-\gamma_{00})+\cos\gamma_{00}} \times\left(\sin(f_{00}-\gamma_{00}) + \frac{\sin f_{00}\cos\gamma_{00}}{1+e_0\cos f_{00}}\right)\left(\frac{a}{a_0}-1\right) \tag{53}$$

Using the obtained ω value of the final orbit, the true anomaly at the satellite point P, f_t can be computed using (4). Equation (49) can also be used to obtain the mean anomaly of the final orbit at the impulse point

$$M_0 \approx M_{00} - \frac{(1-e_0^2)^{3/2}/(2e_0)}{e_0\cos(f_{00}-\gamma_{00})+\cos\gamma_{00}} \times\left(\sin(f_{00}-\gamma_{00}) + \frac{2e_0\sin\gamma_{00}+\sin f_{00}\cos\gamma_{00}}{1+e_0\cos f_{00}}\right) \times\left(\frac{a}{a_0}-1\right) \tag{54}$$

where M_{00} is the mean anomaly of the initial orbit at the initial time.

To simplify the above equations, let's define

$$k_1 = \frac{(1-e_0^2)/(2e_0)}{e_0\cos(f_{00}-\gamma_{00})+\cos\gamma_{00}} \times\left(\sin(f_{00}-\gamma_{00}) + \frac{\sin f_{00}\cos\gamma_{00}}{1+e_0\cos f_{00}}\right) \tag{55a}$$

$$k_2 = \frac{1-e_0^2}{2}\frac{\cos(f_{00}-\gamma_{00})+\cos E_0\cos\gamma_{00}}{e_0\cos(f_{00}-\gamma_{00})+\cos\gamma_{00}} \tag{55b}$$

$$k_3 = \frac{(1-e_0^2)^{3/2}/(2e_0)}{e_0\cos(f_{00}-\gamma_{00})+\cos\gamma_{00}} \times\left(\sin(f_{00}-\gamma_{00}) + \frac{2e_0\sin\gamma_{00}+\sin f_{00}\cos\gamma_{00}}{1+e_0\cos f_{00}}\right) \tag{55c}$$

Then, substituting (52)–(55) into Kepler's equation gives

$$f_s - k_1\left(\frac{a}{a_0}-1\right) - 2\left[e_0 + k_2\left(\frac{a}{a_0}-1\right)\right] \times \sin\left(f_s - k_1\left(\frac{a}{a_0}-1\right)\right) + 2\pi N_R - M_{00} + k_3\left(\frac{a}{a_0}-1\right) = t_K\sqrt{\frac{\mu}{a^3}} \tag{56}$$

where $f_s \triangleq \sin^{-1}(\sin\varphi/\sin i) - \omega_0$ is the Keplerian contribution and does not include the variation of argument of perigee caused by the impulse. Since $a \approx a_0$, the following approximation

$$\sin\left(f_s - k_1\left(\frac{a}{a_0}-1\right)\right) \approx \sin f_s - k_1\left(\frac{a}{a_0}-1\right)\cos f_s \tag{57}$$

can be written. This approximation makes (56) a fifth-order equation in terms of $\sqrt{a}$. By replacing $(a/a_0 - 1)$ with $(1 - a_0/a)$, a cubic equation in terms of $\sqrt{a}$ is obtained from (56). This equation is

$$(f_s + 2\pi N_R - 2e_0\sin f_s - 2k_2\sin f_s - k_1 + k_3 + 2e_0k_1\cos f_s - M_{00})(\sqrt{a})^3 + (2k_2\sin f_s + k_1 - k_3 - 2e_0k_1\cos f_s)a_0(\sqrt{a}) - t_G\sqrt{\mu} = 0 \tag{58}$$

where t_G is obtained using (8).

When considering the linear J_2 perturbation, the cubic equation in terms of $\sqrt{\bar{a}}$ becomes

$$[f_s + 2\pi N_R - 2e_0\sin f_s - 2k_2\sin f_s - k_1 + k_3 + 2e_0k_1\cos f_s - M_{00} - (\dot{M}_{J_2} + \dot{\omega}_{J_2})t_{G_{J_2}}](\sqrt{\bar{a}})^3 + (2k_2\sin f_s + k_1 - k_3 - 2e_0k_1\cos f_s)a_0(\sqrt{\bar{a}}) - t_{G_{J_2}}\sqrt{\mu} = 0 \tag{59}$$

The single-impulse procedure summary for the initial elliptical orbit is as follows.

1) For the Keplerian model, let $f_s \triangleq \sin^{-1}(\sin\varphi/\sin i_0) - \omega_0$. The semimajor axis a_s of the final orbit in then obtained in a closed form using (58), where t_G is obtained using (8).

2) Compute $\dot{\omega}_{J_2}$, $\dot{\Omega}_{J_2}$, and $\dot{M}_{J_2}$ using (15) and the Keplerian semimajor axis a_s. Then $t_{G_{J_2}}$ is obtained using (19).

3) For the perturbed J_2 model, compute the mean semimajor axis $\bar{a}$ of the final orbit using (59).

4) Compute e, ω, and M_0 using (52), (53), (54) and set $i = i_0$ and $\Omega = \Omega_0$. These orbital parameters are then transformed from mean to osculating orbital elements.

5) Compute the single impulse at the initial time using (45).

6) Compute the minimum ΔV_{tot} solution using steps 1 through 5 for all admissible values of N_R.

C. Numerical Method for Single-Impulse Case

The great-circle distance between two points (subscript "1" and "2") on a spherical Earth defined by latitude φ and longitude λ is [16]

$$d = 2R_\oplus\sin^{-1}\sqrt{\sin^2\left(\tfrac{\varphi_2-\varphi_1}{2}\right) + \cos\varphi_1\cos\varphi_2\sin^2\left(\tfrac{\lambda_2-\lambda_1}{2}\right)} \tag{60}$$

A generic Earth site can be observed by ascending and descending ground tracks and in general is located between two successive ascending or descending ground tracks. The minimum distance between the site and the four ground tracks around it can be obtained by numerical methods using (60). The minimum great-circle distance $d_{\min}$ between the site and the four ground tracks of the final orbit can be obtained for any value of the tangential impulse on the initial orbit. By changing the initial impulse, the minimum distance also changes. When the minimum distance is small enough, the ground track can be considered as passing over the site S. The minimum impulse magnitude is then obtained by numerical optimization algorithms (e.g., by the golden section search). In some specific scenarios, only ascending or descending orbits are feasible. To give an example, for a satellite on Sun-synchronous orbit, only the descending ground track part can be used to observe the Earth site.

Moreover, the exact transformation between ECI and ECEF frames must take into account the effects of precession, nutation, sidereal time, and polar motion [1]. With the exact radius vector $\boldsymbol{r}_\oplus$ in ECEF frame, the geodetic latitude φ_d can be obtained [1]. The analytical solutions of the required impulse provided in Sections IV-A and IV-B can then be used as the initial guess to obtain a more accurate geodetic latitude solution by considering ECI-ECEF transformation.

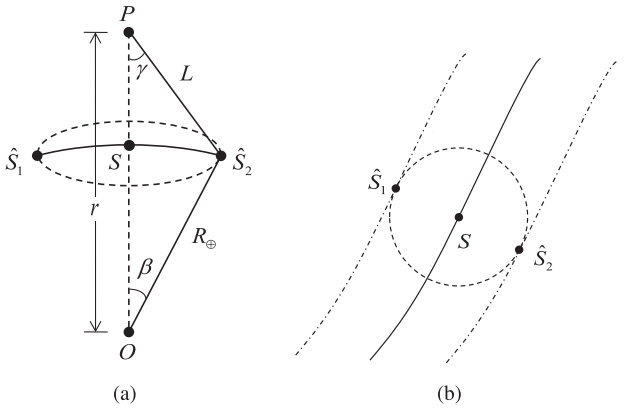

Fig. 3. Geometrical comprehension for conical sensor. (a) From the Earth center. (b) From the ground.

V. IMPULSE METHOD FOR CONICAL SENSOR

The above sections provide analytical approximate solutions of the required impulses and the corresponding time instants for the exact overflight case. When using a conical sensor, if the entire line-of-sight range of the reference ground track covers the target site, then there is no need of orbit maneuver; otherwise, the orbit overflying the site $\hat{S}_1$ or $\hat{S}_2$ (see Fig. 3) satisfies the observation requirement with consequent substantial fuel cost

reduction. For this purpose, the latitudes and longitudes of these two limit sites, $\hat{S}_1$ and $\hat{S}_2$, must be computed. Then the proposed exact overflight method to cover either $\hat{S}_1$ or $\hat{S}_2$ can be adopted. Let $\hat{S}$ be the site associated with less maneuver cost.

A conical sensor is assumed to simplify the analysis for the entire line-of-sight range, even though the qualities of the pass for direct and slewing observations are different. However, the proposed method for conical sensor can be extended to an additional cone including slewing observation. Actually, for most high-resolution Earth-observation satellites (e.g., French Pléiades satellites), the field-of-view angle without slewing is small (it is only 1.65° for Pléiades satellites, whose ground swath is about 20 km at an altitude of 695 km). This means that, in most cases, the satellite needs to slew in Earth-observation missions.

Let $\gamma_{\max}$ be the maximum half-angle of the conical sensor; then the maximum angle $\beta_{\max}$ at the Earth's center is obtained using the law of sines [see Fig. 3(a)]

$$\beta_{\max} = \arcsin\left(\frac{r\sin\gamma_{\max}}{R_\oplus}\right) - \gamma_{\max} \tag{61}$$

while the slant range is

$$L_{\max} = \frac{\sin\beta_{\max}}{\sin\gamma_{\max}} R_\oplus \tag{62}$$

The position vectors of $\hat{S}_1$ and $\hat{S}_2$ in the ECI frame are then obtained by rotating the position vector of S by the angles $\pm\beta$ with respect to the "$\boldsymbol{h} \times \boldsymbol{r}$" direction,

$$\boldsymbol{r}_{\hat{S}_1,\hat{S}_2} = R_{\boldsymbol{h}\times\boldsymbol{r}}(\pm\beta_{\max})\,\boldsymbol{r}\,\frac{R_\oplus}{r} \tag{63}$$

By transforming the position vectors from ECI to ECEF and using the same GMST of S, the latitudes and longitudes of $\hat{S}_1$ and $\hat{S}_2$ are then obtained.

Equation (61) shows that the angle $\beta_{\max}$ is a function of the radius r. This means that the above method is approximated because the orbital radius of trajectory passing over $\hat{S}$ is not equal to that passing over S. To correct this approximated solution, an algorithm iterating on the radius of $\hat{S}$ can be used to obtain latitudes and longitudes of $\hat{S}$. Our preliminary results show that no more than two iterations are needed to obtain a sufficiently accurate solution. This exact overflight solution to cover $\hat{S}$ is then used to compute the required impulses and the corresponding time instants.

When using these impulses on the reference orbit, the maneuvering ground track is obtained. The minimum ground distance $d_{\min}$, between the ground track and the target site S, can be then obtained using a numerical iterative algorithm. Once this distance is computed, the "true" angle β is simply

$$\beta = \frac{d_{\min}}{R_\oplus} \tag{64}$$

The law of sines gives

$$\frac{\sin(\gamma+\beta)}{r} = \frac{\sin\gamma}{R_\oplus} = \frac{\sin\beta}{L} \tag{65}$$

which allows us to compute the required sensor half-angle γ

$$\tan\gamma = \frac{R_\oplus\sin\beta}{r - R_\oplus\cos\beta} \tag{66}$$

and the "true" slant range

$$L = R_\oplus\frac{\sin\beta}{\sin\gamma} \tag{67}$$

Therefore, when impulse and impulse time instants are computed, the required sensor half-angle γ and the slant range L are provided by (66) and (67), respectively. If the γ angle for the reference ground track of the initial orbit is less than its maximum value ($\gamma < \gamma_{\max}$), then there is no need to apply impulses. Otherwise, the ground track correction is used to compute the "true" slant range L and the angle γ, which would be close to its maximum value $\gamma_{\max}$.

VI. NUMERICAL EXAMPLES

Four numerical examples to validate the proposed methodology are presented:

1) initial and final circular, two-impulses;
2) initial elliptical, final circular, two-impulses;
3) initial circular, final elliptical, single-impulse;
4) initial and final elliptical, single-impulse.

July 1, 2015 at 08:00:00 is the selected UTC initial time. At this time the GMST is $\alpha_{G0} = 0.681733$ rad. The city of Wenchuan, which experienced a strong earthquake in 2008, is selected as the Earth site. The geographical coordinates of Wenchuan are $\lambda = 103.4°$ and $\varphi = 31°$. The conical sensor has the maximum half-angle of $\gamma_{\max} = 30°$.

The results obtained by the proposed method are shown in the four cases. In the ground-track figures, the dotted line indicates the sensor range while the dashed line indicates the reference ground track without maneuvers, and the solid line indicates the maneuvering ground track. The star marker indicates the target Earth site S, and the square marker indicates the new site $\hat{S}$ for conical sensor. The nonlinear J_2 perturbed orbit propagation is numerically obtained using Matlab function ode45. Then, latitude and longitude in ground tracks are obtained using (2) and (3), respectively. In the following tables, "D" and "A" indicate descending and ascending ground tracks, respectively.

Moreover, Pareto plots are provided for two cases: 1) two objectives: time to overflight and fuel cost; 2) three objectives: time to overflight, slant range, and fuel cost. Both exact overflight and conical sensor cases are considered. For each admissible day, the minimum-fuel solution and the corresponding slant range are obtained using the proposed method.

TABLE I
Case 1: Two-Impulses, Initial and Final Circular, Exact Overflight, $t_1 = 0$ s, where "D" and "A" indicate Descending and Ascending Ground Tracks, respectively

Types	Days	ΔV_1 (km/s)	ΔV_2 (km/s)	ΔV_{tot} (km/s)	t_2 (s)	$d_{\min}$ (km)	t_S (s)	L (km)	γ (°)
D	1	–0.045368	–0.045637	0.091005	2729.1	1.5	21.460	234.9	0.37
A	1	0.164651	0.161113	0.325764	2968.8	3.8	8.877	1013.8	0.22
D	2	0.003186	0.003184	0.006370	2781.1	1.4	24 + 21.452	404.0	0.20
A	2	0.014935	0.014905	0.029840	2793.9	1.4	24 + 8.883	451.6	0.18
D	3	–0.010070	–0.010083	0.020153	2766.7	1.3	48 + 21.459	357.2	0.21
A	3	–0.006328	–0.006333	0.012662	2770.8	1.4	48 + 8.889	376.0	0.21
D	4	0.004479	0.004477	0.008956	2782.5	1.6	72 + 21.452	408.5	0.22
A	4	0.009418	0.009407	0.018825	2787.9	1.4	72 + 8.882	431.6	0.18
D	5	–0.003626	–0.003628	0.007254	2773.7	1.1	96 + 21.458	421.5	0.15
A	5	–0.000818	–0.000818	0.001636	2776.7	1.3	96 + 8.888	395.2	0.19
D	6	0.004893	0.004890	0.009783	2782.9	1.6	120 + 21.451	409.8	0.22
A	6	–0.007195	–0.007201	0.014396	2769.8	3.9	120 + 8.895	372.5	0.60
D	7	0.000922	0.000922	0.001844	2776.6	1.1	144 + 21.457	389.2	0.17
A	7	0.001229	0.001229	0.002458	2779.0	1.3	144 + 8.888	402.1	0.19

A. Case 1: Initial and Final Circular, Two-Impulses

The initial orbit is Sun-synchronous with orbital elements $a_0 = R_\oplus + 400$ km, $e_0 = 0$, $i_0 = 97.0346^\circ$, $\Omega_0 = 280^\circ$, and $u_{00} = 0^\circ$. The observation time limit is selected as one day. The descending (D) ground track is selected.

For the exact overflight case, the mean semimajor axis of the final orbit (J_2 perturbation included) is $\bar{a} = 6{,}610.234$ km, computed using (27). Then, the osculating semimajor axis of the final orbit is $a = 6{,}620.078$ km. The two impulses are $\Delta V_1 = -0.045368$ km/s and $\Delta V_2 = -0.045637$ km/s, with a total cost of $\Delta V_{\text{tot}} = 0.091005$ km/s. The minimum cost is obtained with $N_R = 14$, which is the next larger integer to $N_{R\text{opt}} = 13.46$ obtained using (14). The first impulse occurs at the initial time while the second impulse occurs at $t_2 = t_H = 2{,}729.2$ s. The ground tracks for the reference and maneuvering orbits are plotted in Fig. 4(a).

For the conical sensor case, the geographical coordinates of $\hat{S}$ are $\hat{\lambda} = 101.842^\circ$ and $\hat{\varphi} = 31.184^\circ$, and the total cost is $\Delta V_{\text{tot}} = 0.078057$ km/s. The sensor angle is $\gamma = 30.2^\circ$, which is near to its maximum value. The ground tracks are plotted in Fig. 4(b). Compared with the exact overflight case, the fuel cost of the conical sensor case is reduced by 14.2%; however, the slant range increases by 27.5%.

Table I provides time to overflight t_S, impulse ΔV, maneuver time instant t_2, overflight distance error $d_{\min}$, slant range L, and sensor angle γ for the exact overflight case with different observation time limits and for ascending and descending orbits. The first impulse occurs at the initial time while $t_2 = t_H$ indicates the second impulse time.

Table II provides the results, including the geographical coordinates of $\hat{S}$, for the conical sensor case.

The feasible solutions listed in Tables I and II are divided into two categories: dominated and nondominated points. For the two-objective case, these points are given in Fig. 5(a), showing that the conical constraint uses less fuel than the exact overflight constraint. In addition, the Pareto front is obtained using the MATLAB interpolation function "interp1" for the nondominated points.

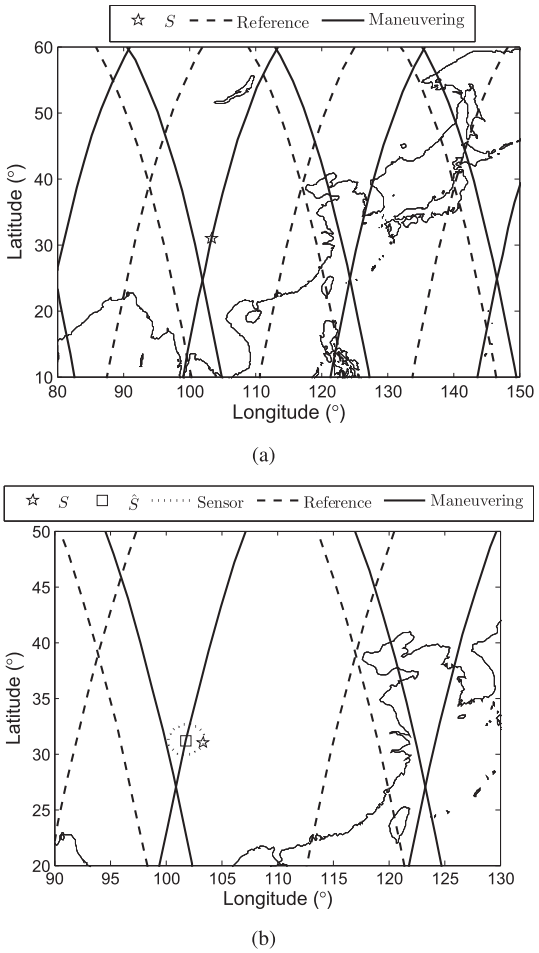

Fig. 4. Ground tracks for two-impulse initial and final circular orbits. (a) Exact overflight. (b) Conical sensor.

TABLE II
Case 1: Two-Impulses, Initial and Final Circular, Conical Sensor, $t_1 = 0$ s

Types	Days	ΔV_1 (km/s)	ΔV_2 (km/s)	ΔV_{tot} (km/s)	t_2 (s)	$d_{\min}$ (km)	t_S (h)	L (km)	γ (°)	$(\hat{\varphi}, \hat{\lambda})$ (°)
D	1	–0.038929	–0.039127	0.078057	2735.9	150.7	21.564	299.5	30.2	(31.184, 101.842)
A	1	0.112056	0.110418	0.222474	2905.0	492.0	8.533	963.5	30.7	(31.534, 108.532)
D	2	0	0	0	0	159.9	24 + 21.341	425.9	22.0	N/A
A	2	0.007985	0.007976	0.015961	2786.3	249.6	24 + 8.708	498.6	30.0	(31.299, 105.997)
D	3	–0.007330	–0.007337	0.014668	2769.7	209.7	48 + 21.605	425.5	29.5	(31.386, 101.245)
A	3	–0.002810	–0.002811	0.005621	2774.6	221.4	48 + 9.043	450.4	29.4	(30.695, 101.118)
D	4	0.002201	0.002201	0.004402	2780.0	235.8	72 + 21.288	468.4	30.2	(30.670, 105.828)
A	4	0.006641	0.006635	0.013276	2784.9	247.5	72 + 8.709	493.1	30.1	(31.292, 105.975)
D	5	–0.001909	–0.001910	0.003819	2775.5	222.6	96 + 21.613	448.7	29.7	(31.267, 101.084)
A	5	0	0	0	0	95.8	96 + 8.954	410.1	13.5	N/A
D	6	0.003354	0.003352	0.006706	2781.2	241.8	120 + 21.283	475.0	30.6	(30.666, 105.889)
A	6	–0.005643	–0.005647	0.011291	2771.5	224.4	120 + 9.049	442.9	30.4	(30.691, 101.114)
D	7	0	0	0	0	168.6	144 + 21.575	429.2	23.1	N/A
A	7	0	0	0	0	205.1	144 + 8.743	450.4	27.1	N/A

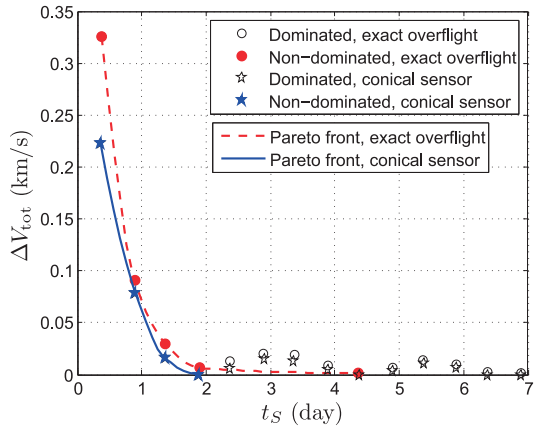

(a)

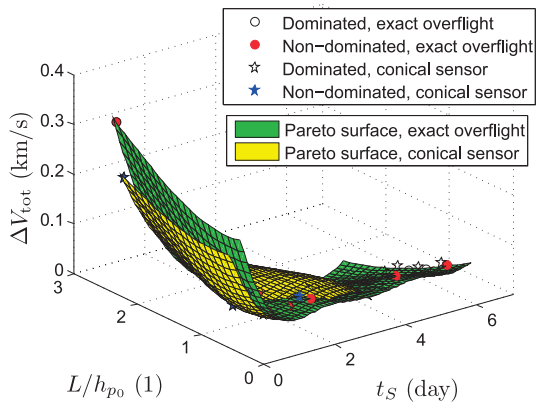

(b)

Fig. 5. Pareto plots for two-impulse initial and final circular orbits. (a) Two objectives. (b) Three objectives.

For the three-objective case, the points of dominated and nondominated solutions are given in Fig. 5(b). For the nondominated solutions, the MATLAB interpolation function "griddata" is used to produce the Pareto surface. To obtain the uniformed value, the normalized slant range is L/h_{p_0}($h_{p_0} = 400$ km is the perigee height of the initial orbit). The Pareto surface is plotted in Fig. 5(b). Note that the Pareto plots are interpolation results; there may be no corresponding solution on the Pareto surface, e.g., the time to overflight can only change slightly because of the Earth rotation (see t_S values in Tables I and II).

B. Case 2: Initial Elliptical, Final Circular, Two-Impulses

The selected initial elliptical orbit has perigee radius $r_p = R_\oplus + 400$ km, apogee radius $r_a = R_\oplus + 1000$ km, $i_0 = 97.0346°$, $\omega_0 = 0°$, $\Omega_0 = 280°$, and $f_{00} = 60°$. The initial eccentricity is $e_0 = 0.042384$. The observation time is selected as one day. The exact overflight case is considered. The initial coasting time under J_2 effects is $t_{\text{coasting}} = 2,065.6$ s.

When selecting descending ground track, the mean semimajor axis of the final orbit is $\bar{a} = 7{,}371.676$ km, computed using (31). The two impulses are $\Delta V_1 = 0.155486$ km/s and $\Delta V_2 = -0.003960$ km/s, with a total cost of $\Delta V_{\text{tot}} = 0.159446$ km/s. The first impulse occurs at $t_1 = t_{\text{coasting}} = 2{,}065.6$ s and the second impulse at $t_2 = t_{\text{coasting}} + t_H = 5{,}226.5$ s.

When selecting ascending ground track, the mean semimajor axis of the final orbit is $\bar{a} = 7{,}548.458$ km. The two impulses are $\Delta V_1 = 0.198771$ km/s and $\Delta V_2 = 0.039116$ km/s, with a total cost of $\Delta V_{\text{tot}} = 0.237887$ km/s. The first impulse occurs at $t_1 = 2,065.6$ s and the second impulse at $t_2 = 5{,}283.3$ s. The ground tracks are plotted in Fig. 6.

Table III provides the results obtained for the exact overflight case. In this table $t_1 = t_{\text{coasting}}$ is the first impulse time and $t_2 = t_{\text{coasting}} + t_H$ is the second impulse time. The values of t_1 are the same for all cases. The results show that all values of ΔV_{tot} are very close except the ascending case with one day limit. This is because the minimum cost for a final circular orbit is $\Delta V_{\text{tot}} = 0.159444$ km/s using the J_2 model and the corresponding latitude is equal to the apogee latitude (see Section III-B). The fuel costs for different days are almost the same even though the final circular orbit radii are different (see Fig. 2). Therefore, compared with the exact overflight case, the fuel cost cannot be reduced for the conical sensor

TABLE III
Case 2: Two-Impulses, Initial Elliptical and Final Circular, Exact Overflight, $t_1 = 2{,}065.6$ s

Types	Days	ΔV_1 (km/s)	ΔV_2 (km/s)	ΔV_{tot} (km/s)	t_2 (s)	$d_{\min}$ (km)	t_S (h)	L (km)	γ (°)
D	1	0.155486	–0.003960	0.159446	5226.5	0.4	21.438	1000.1	0.02
A	1	0.198771	0.039116	0.237887	5283.3	0.4	8.879	1171.9	0.02
D	2	0.140757	–0.018734	0.159491	5207.7	2.3	24 + 21.426	942.5	0.14
A	2	0.145415	–0.014055	0.159470	5213.6	2.1	24 + 8.867	955.8	0.13
D	3	0.136387	–0.023129	0.159516	5202.1	4.3	48 + 21.423	925.2	0.27
A	3	0.138051	–0.021455	0.159506	5204.2	4.1	48 + 8.853	926.6	0.25
D	4	0.157215	–0.002229	0.159444	5228.7	1.1	72 + 21.388	1008.3	0.06
A	4	0.135123	–0.024401	0.159524	5200.5	6.0	72 + 8.840	915.2	0.38
D	5	0.151214	–0.008239	0.159453	5221.0	3.1	96 + 21.356	984.3	0.18
A	5	0.153923	–0.005524	0.159448	5224.5	2.9	96 + 8.816	990.0	0.17
D	6	0.147277	–0.012187	0.159464	5216.0	5.1	120 + 21.363	968.6	0.30
A	6	0.149085	–0.010373	0.159458	5218.3	4.8	120 + 8.803	970.8	0.28
D	7	0.157430	–0.002014	0.159444	5229.0	2.0	144 + 21.338	1009.3	0.11
A	7	0.145785	–0.013684	0.159469	5214.1	6.7	144 + 8.790	957.8	0.40

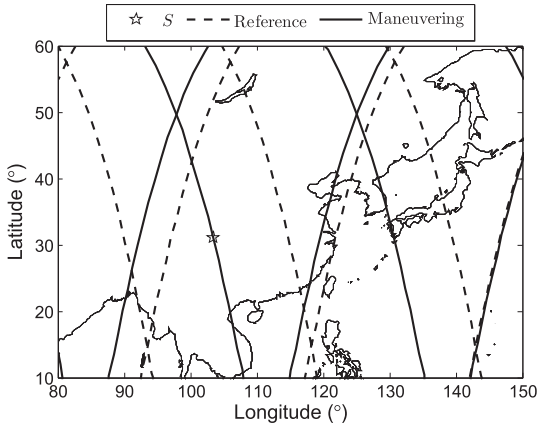

Fig. 6. Ground tracks for two-impulse initial elliptical and final circular orbits, exact overflight.

case, unless the impulses are not needed when the reference ground track with conical sensor can directly cover the target site. Therefore, the ground-track plot for conical sensor and the Pareto plots are not provided for case 2.

C. Case 3: Initial Circular, Final Elliptical, Single-Impulse

For this case the initial orbital elements are the same as those in Section VI-A. The observation time constraint is one day, and the descending ground track is selected.

For the exact overflight case, the mean semimajor axes of the final orbit for $\Delta V < 0$ and $\Delta V > 0$ are $\bar{a} = 6{,}611.851$ km and $\bar{a} = 6{,}937.616$ km, respectively. The corresponding impulses are –0.091417 km/s and 0.092883 km/s, respectively. However, the perigee radius for the solution with $\bar{a} = 6{,}611.851$ km is less than 200 km, thus $\bar{a} = 6{,}937.616$ km is selected. Finally, the single impulse at the initial time is $\Delta V_1 = 0.092883$ km/s. The ground tracks for the reference and maneuvering orbits are plotted in Fig. 7(a).

For the conical sensor case, the geographical coordinates of $\hat{S}$ are $\hat{\lambda} = 107.080°$ and $\hat{\varphi} = 30.491°$, and the total cost is 0.063320 km/s. Compared with the exact

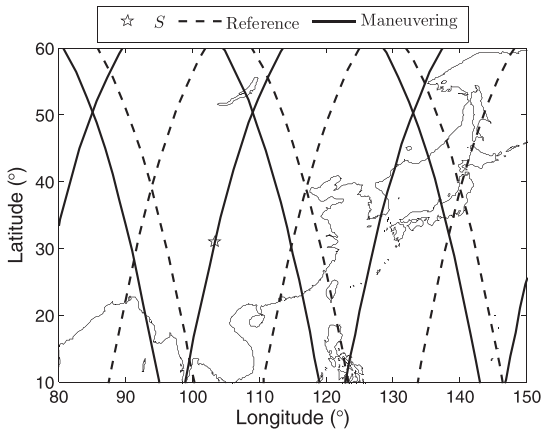

(a)

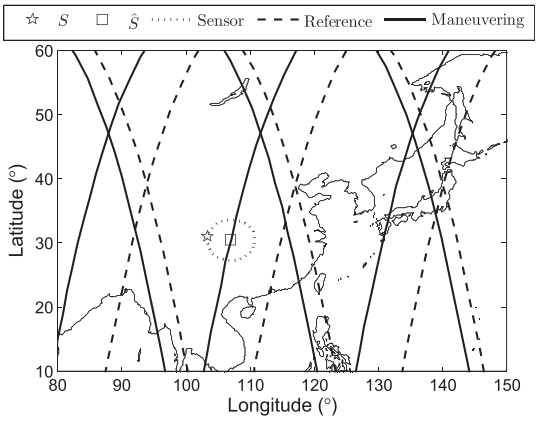

(b)

Fig. 7. Ground tracks for single-impulse initial circular and final elliptical orbits. (a) Exact overflight. (b) Conical sensor.

overflight case, a 31.8% fuel saving is obtained for the conical sensor case while the slant range increases by only 0.5%. The ground tracks are plotted in Fig. 7(b).

Tables IV and V provide the results for the exact overflight case and for the conical sensor case, respectively. The single impulse is at the initial time. For the initial circular, the total cost values by the

TABLE IV
Case 3: Single-Impulse, Initial Circular and Final Elliptical, Exact Overflight, $t_1 = 0$ s

Types	Days	ΔV_1 (km/s)	$d_{\min}$ (km)	t_S (h)	L (km)	γ (°)
D	1	0.092883	0.3	21.449	709.8	0.02
A	1	0.305649	0.7	8.880	478.4	0.09
D	2	0.006358	0.9	24 + 21.453	414.2	0.12
A	2	0.029629	0.2	24 + 8.883	408.6	0.03
D	3	–0.020206	1.4	48 + 21.457	324.0	0.25
A	3	–0.012672	0.8	48 + 8.889	393.0	0.12
D	4	0.008943	0.4	72 + 21.452	423.6	0.06
A	4	0.018777	0.3	72 + 8.883	407.4	0.04
D	5	–0.007279	1.3	96 + 21.456	367.3	0.20
A	5	–0.001647	0.8	96 + 8.888	379.1	0.11
D	6	0.009771	0.1	120 + 21.452	426.9	0.02
A	6	–0.014453	1.3	120 + 8.893	388.2	0.20
D	7	–0.001860	0.9	144 + 21.456	385.9	0.13
A	7	0.002448	0.7	144 + 8.888	399.6	0.10

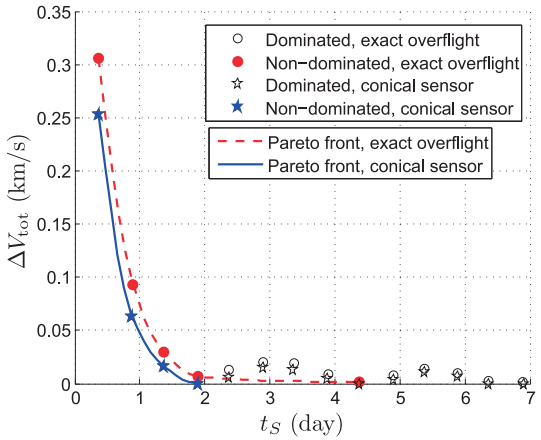

(a)

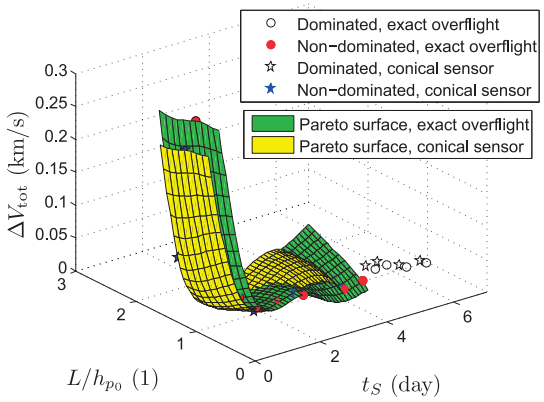

(b)

Fig. 8. Pareto plots for single-impulse initial circular and final elliptical orbits. (a) Two objectives. (b) Three objectives.

single-impulse method with an elliptical final orbit are close to those by the two-impulse method with a circular final orbit.

Using the results in Tables IV and V, the Pareto plots for case 3 are provided in Fig. 8.

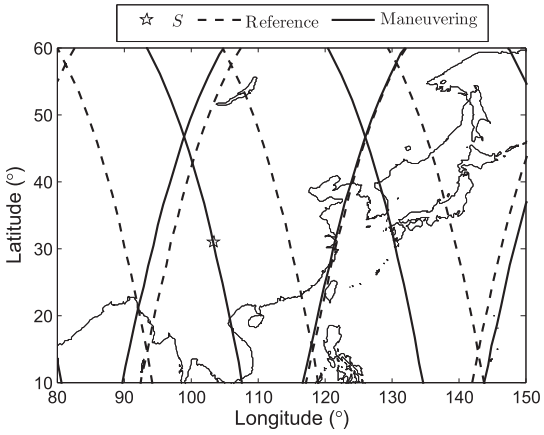

(a)

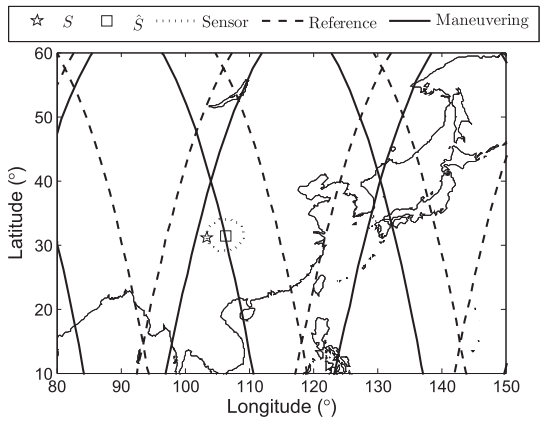

(b)

Fig. 9. Ground tracks for single-impulse initial and final elliptical orbits. (a) Exact overflight. (b) Conical sensor.

D. Case 4: Initial and Final Elliptical, Single-Impulse

For this case the initial orbital elements are the same as those in Section VI-B. The observation time constraint is one day and the ascending ground track is selected.

For the exact overflight case, the mean semimajor axis of the final orbit is $\bar{a} = 7{,}506.587$ km. The osculating semimajor axis of the final orbit is $a = 7{,}502.599$ km. The single impulse is $\Delta V_1 = 0.204818$ km/s. The ground tracks for the reference and maneuvering orbits are plotted in Fig. 9(a).

For the conical sensor case, the geographical coordinates of $\hat{S}$ are $\hat{\lambda}$= 106.296° and $\hat{\varphi}$= 31.320°, while the single impulse is $\Delta V_1 = 0.154274$ km/s. Compared with the exact overflight case, the conical sensor case saves 24.7% of the fuel but the slant range increases by 14.5%. The ground tracks are plotted in Fig. 9(b).

Tables VI and VII provide the results for the exact overflight case and for the conical sensor case, respectively. Again, the single impulse is at the initial time.

Using the results in Tables VI and VII, there are only three nondominated solutions for both two-objective and three-objective cases. The Pareto plots for case 4 are given in Fig. 10.

TABLE V
Case 3: Single-Impulse, Initial Circular and Final Elliptical, Conical Sensor, $t_1 = 0$ s

Types	Days	ΔV_1 (km/s)	$d_{\min}$ (km)	t_S (h)	L (km)	γ (°)	$(\hat{\varphi}, \hat{\lambda})$ (°)
D	1	0.063320	356.9	21.200	713.2	30.0	(30.491107.080)
A	1	0.253079	278.0	8.684	549.1	30.4	(31.322106.308)
D	2	0	159.9	24 + 21.341	425.9	22.0	N/A
A	2	0.016497	237.8	24 + 8.717	472.8	30.2	(31.284, 105.883)
D	3	–0.015022	195.4	48 + 21.595	396.1	29.5	(31.234101.350)
A	3	–0.005321	230.4	48 + 9.049	461.9	29.9	(30.687101.021)
D	4	0.004337	238.4	72 + 21.286	476.1	30.0	(30.672,1.05860)
A	4	0.013462	237.3	72 + 8.716	473.1	30.0	(31.284, 105.876)
D	5	–0.003879	218.2	96 + 21.610	440.6	29.7	(31.267, 101.115)
A	5	0	95.8	96 + 8.954	410.1	13.5	N/A
D	6	0.006587	249.6	120 + 21.277	489.0	30.7	(30.653105.978)
A	6	–0.011239	228.8	120 + 9.052	456.1	30.1	(30.689101.044)
D	7	0	168.6	144 + 21.575	429.2	23.1	N/A
A	7	0	205.1	144 + 8.743	450.4	27.1	N/A

TABLE VI
Case 4: Single-Impulse, Initial and Final Elliptical, Exact Overflight, $t_1 = 0$ s

Types	Days	ΔV_1 (km/s)	$d_{\min}$ (km)	t_S (h)	L (km)	γ (°)
D	1	–0.048336	1.1	21.448	960.2	0.07
A	1	0.204818	4.4	8.882	483.0	0.53
D	2	0.025368	2.4	24 + 21.435	1037.4	0.13
A	2	–0.000268	1.5	24 + 8.872	453.2	0.18
D	3	–0.010196	4.2	48 + 21.431	967.8	0.26
A	3	–0.032548	1.7	48 + 8.867	459.7	0.21
D	4	0.015660	4.4	72 + 21.417	1034.6	0.24
A	4	0.003790	4.5	72 + 8.851	473.0	0.54
D	5	–0.003307	8.4	96 + 21.415	995.2	0.48
A	5	–0.014637	2.6	96 + 8.847	483.6	0.31
D	6	0.012526	4.1	120 + 21.398	1040.7	0.23
A	6	0.004828	7.3	120 + 8.830	495.3	0.85
D	7	–0.000460	9.1	144 + 21.396	1010.9	0.52
A	7	–0.007980	5.0	144 + 8.827	508.0	0.57

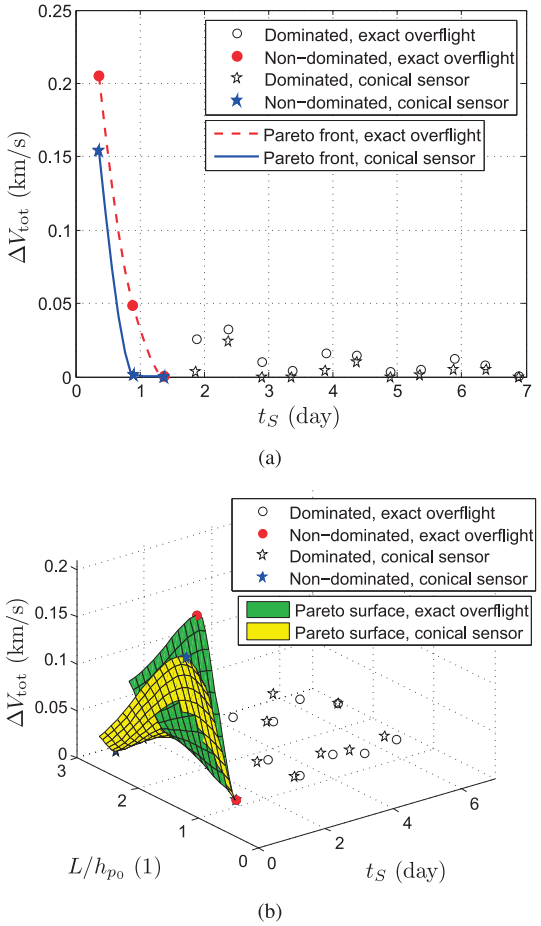

Fig. 10. Pareto plots for single-impulse initial and final elliptical orbits. (a) Two objectives. (b) Three objectives.

For the exact overflight case, Tables I, III, IV, and VI show that all overflight distance errors ($d_{\min}$) are less than five km in three days. As time increases to seven days, the values for $d_{\min}$ are also less than five km for the initial circular orbit but they increase to about ten km for the initial elliptic orbit. For the conical sensor case, Tables II, V, and VII show that the impulse is not needed in some cases since the required sensor half-angle γ for the reference ground track is less than $\gamma_{\max} = 30°$.

Compared with the exact overflight case, the conical sensor case needs less fuel and greater slant range in most cases, except for the two-impulse method for initial elliptical orbit. The values of t_S for the exact overflight and conical sensor cases are slightly different. In general the optimization of a single parameter (t_S or L or ΔV_{tot}) does not always improve the others. Trading between these three objectives implicitly defines a Pareto surface (see Figs. 5, 8, and 10). On this surface users can identify the specific optimal solution based on the mission and observation requirements.

All the computations are performed using MATLAB on a Dual-Core Pentium with 3.06 GHz CPU, 2 GB RAM, and Windows 7. For the exact overflight case, the computational time for the required impulses and corresponding time instants is about 0.13 s (includes the computational time 0.09 s for transforming mean into osculating elements using the method in [14], whereas for the conic sensor case, the computational time is about 0.28 s.

TABLE VII
Case 4: Single-Impulse, Initial and Final Elliptical, Conical Sensor, $t_1 = 0$ s

Types	Days	ΔV_1 (km/s)	$d_{\min}$ (km)	t_S (h)	L (km)	γ (°)	$(\hat{\varphi}, \hat{\lambda})$ (°)
D	1	–0.001456	567.6	21.846	1143.6	29.7	(31.594, 97.438)
A	1	0.154274	275.3	8.685	553.1	29.8	(31.320, 106.296)
D	2	0.002981	583.0	24 + 21.026	1173.1	29.8	(30.105, 109.418)
A	2	0	3.9	24 + 8.876	453.2	0.49	N/A
D	3	0	408.4	48 + 21.715	1081.9	22.2	N/A
A	3	–0.024386	264.9	48 + 9.054	534.7	29.7	(30.628, 100.641)
D	4	0.004371	605.4	72 + 20.992	1201.7	30.2	(30.061, 109.679)
A	4	0	181.3	72 + 8.727	509.7	20.8	N/A
D	5	0	230.9	96 + 21.571	1033.0	12.9	N/A
A	5	–0.010018	276.7	96 + 9.043	561.0	29.5	(30.608, 100.504)
D	6	0.005075	606.1	120 + 20.972	1213.3	29.9	(30.052, 109.720)
A	6	0.000852	302.3	120 + 8.623	588.0	30.9	(31.354, 106.492)
D	7	0	52.9	144 + 21.427	1013.6	2.99	N/A
A	7	–0.004694	285.2	144 + 9.030	586.4	29.1	(30.590, 100.380)

VII. CONCLUSIONS

This paper provides approximate analytical solutions to observe an assigned Earth site for both exact overflight and conical sensor cases by modifying the ground track using single and double tangential-impulse maneuvers. Four cases, including a two-impulse approach with circular final orbit and a single-impulse approach with elliptical final orbit starting from circular and elliptical initial orbits, are presented. The approximate analytical solutions are obtained by considering the linear J_2 perturbation. Solutions for descending and ascending ground tracks are provided, separately. These analytical solutions provide the overflight distance error between the assigned Earth site and the ground track less than five km in three days. For an initial circular orbit, the total costs obtained using single and double impulse methods are close. Compared with the exact overflight case, the conical sensor case needs less fuel and greater slant range in most cases except for the two-impulse method for initial elliptical orbit. In addition, considering that the conical sensor trading between different objectives defines a Pareto surface, this allows users to choose how they wish to trade these quantities.

The analytical solutions provided using geocentric latitudes can also be adopted as an initial guess in higher precision models using geodetic latitudes and Earth gravitation models better than the linear J_2. The proposed methods are particularly suitable to Sun-synchronous observation satellites only using the descending ground track part. The provided analytical solutions can be used for fast computations in responsive space missions which require emergency observation of an assigned Earth site.

APPENDIX A. CLOSED-FORM SOLUTIONS FOR DEPRESSED CUBIC POLYNOMIAL

For the following depressed cubic equation

$$x^3 + c_1 x + c_0 = 0 \tag{68}$$

by using Vieta's substitution [17]

$$x = y - \frac{c_1}{3y} \tag{69}$$

a quadratic equation of y^3 is obtained as

$$y^3 + c_0 - \frac{c_1^3}{27y^3} = 0 \rightarrow y^6 + c_0 y^3 - \frac{c_1^3}{27} = 0 \tag{70}$$

which yields

$$y^3 = -\frac{1}{2}c_0 \pm \sqrt{\frac{1}{4}c_0^2 + \frac{c_1^3}{27}} \tag{71}$$

There are, therefore six solutions (three pairs) for y. However, each pair is equal when using (69) for x, so there are three solutions to the original depressed cubic equation (68).

ACKNOWLEDGMENT

The authors would like to thank Rose Sauser for generously reviewing this manuscript for consistency and formalism.

REFERENCES

[1] Vallado, D. A.
Fundamentals of Astrodynamics and Applications, 3rd ed. Torrance, CA: Microcosm Press, 2007.

[2] Aorpimai, M., and Palmer, P. L.
Repeat-groundtrack orbit acquisition and maintenance for earth-observation satellites.
Journal of Guidance, Control, and Dynamics, **30**, 3 (2007), 654–659.

[3] Sengupta, P., Vadali, S. R., and Alfriend, K. T.
Satellite orbit design and maintenance for terrestrial coverage.
Journal of Spacecraft and Rockets, **47**, 1 (2010), 177–187.

[4] Mortari, D., Wilkins, M. P., and Bruccoleri, C.
The Flower Constellations.
The Journal of the Astronautical Sciences, **52**, 1–2 (2004), 107–127.

[5] Mortari, D., and Wilkins, M. P.
The Flower Constellation set theory Part I: Compatibility and phasing.

IEEE Transactions on Aerospace and Electronic Systems, **44**, 3 (2008), 953–963.

[6] Casanova, D., Avendaño, M. E., and Mortari, D.
Design of Flower Constellations using necklaces.
IEEE Transactions on Aerospace and Electronic Systems, **50**, 2 (2014), 1347–1358.

[7] Abdelkhalik, O., and Mortari, D.
Orbit design for ground surveillance using genetic algorithms.
Journal of Guidance, Control, and Dynamics, **29**, 5 (2006), 1231–1235.

[8] Abdelkhalik, O.
Initial orbit design from ground track points.
Journal of Spacecraft and Rockets, **47**, 1 (2010), 202–205.

[9] Zhu, K. J., Li, J. F., and Baoyin, H. X.
Satellite scheduling considering maximum observation coverage time and minimum orbital transfer fuel cost.
Acta Astronautica, **26**, 1 (2010), 220–229.

[10] Co, T. C., Zagaris, C., and Black, J. T.
Responsive satellites through ground track manipulation using existing technology.
Journal of Spacecraft and Rockets, **50**, 1 (2013), 206–216.

[11] Co, T. C., and Black, J. T.
Responsiveness in low orbits using electric propulsion.
Journal of Spacecraft and Rockets, **51**, 3 (2014), 938–945.

[12] Zhang, J., Li, H. Y., Luo, Y. Z., and Tang, G. J.
Effects of in-track maneuver on the ground track of near-circular orbits.
Journal of Guidance, Control, and Dynamics, **37**, 4 (2014), 1373–1378.

[13] Pontani, M.
Simple method to determine globally optimal orbital transfers.
Journal of Guidance, Control, and Dynamics, **32**, 3 (2009), 899–914.

[14] Gim, D., and Alfriend, K. T.
State transition matrix of relative motion for the perturbed noncircular reference orbit.
Journal of Guidance, Control, and Dynamics, **26**, 6 (2003), 956–971.

[15] Zhang, G., Zhou, D., and Mortari, D.
Optimal two-impulse rendezvous using constrained multiple-revolution lambert solutions.
Celestial Mechanics and Dynamical Astronomy, **110**, 4 (2011), 305–317.

[16] Sinnott, R.W.
Virtues of the haversine.
Sky and Telescope, **68**, 2 (1984), 159.

[17] Birkhoff G., and MacLane, S.
A Survey of Modern Algebra. New York: Macmillan, 1965, p. 106.

Gang Zhang received the B.S. degree from the School of Mathematics at Jilin University, Changchun, China, in 2007, and the Ph.D. degree in aerospace engineering from Harbin Institute of Technology, Harbin, China, in 2012.

He is currently an Associate Professor at the Research Center of Satellite Technology, Harbin Institute of Technology. His research areas are orbit mechanics, orbit rendezvous, and trajectory optimization.

Xibin Cao received the Ph.D. degree from the Harbin Institute of Technology, Harbin, China, in 1991.

Since 1991, he has been in the Department of Astronautics and Mechanics, Harbin Institute of Technology. Since 1999, he has been a Professor and Director of the Research Center of Satellite Technology, Harbin Institute of Technology. His current research interests include microsatellite design methodology and system simulation of small satellite.

Daniele Mortari (M'05—SM'12—F'16) received his "Dottore" degree in Nuclear Engineering from "La Sapienza" University of Rome in 1981.

He is Professor of Aerospace Engineering at Texas A&M University, College Station, TX. He is active in the fields of orbital mechanics, attitude determination, satellite constellations, star navigation, and sensor data processing.

Dott. Mortari is the author of more than 250 papers. He received two NASA Group Achievement awards (for San Marco V mission and Inertial Stellar Compass), the Spacecraft Technology Center Award (for StarNav I experiment on STS-107), and the prestigious 2007 IEEE Judith A. Resnik Award for the Flower Constellations. He is an AAS Fellow, AIAA Associate Fellow, Associate Editor of *IEEE Transactions on Aerospace and Electronic Systems*, and Honorary Member of IEEE-AESS Space Systems Technical Panel. He has been IEEE Distinguished Speaker and member of the AAS Space Flight Mechanics Technical Committee.